Atomic Spectroscopy

Article

Data Processing Strategies for the Improved Analysis of Solder by Electrothermal Vaporization (ETV) Coupled to ICPOES

Kate Moghadam and Diane Beauchemin*

Department of Chemistry, Queen's University, Kingston, ON, K7L 3N6, Canada

Received: *February 13, 2024;* ***Revised:*** *May 02, 2024;* ***Accepted:*** *May 02, 2024;* ***Available online:*** *May 02, 2024.*

DOI: 10.46770/AS.2024.032

ABSTRACT: Applications of electrothermal vaporization coupled to inductively coupled plasma optical emission spectrometry (ETV-ICPOES) may require offline, and often manual, processing for data compilation and optimization. Techniques for data processing have traditionally applied internal standardization and some form of correction (*e.g.*, blank subtraction) to compensate for positive bias from the background. However, a blank may not always be easily obtained in applications of solid-sampling research, and in some cases, degrade detection limits and signal integrations. In this work, several data processing techniques are evaluated, after point-by-point internal standardization with an Ar emission line, for the sensitive and accurate analysis of solder by ETV-ICPOES: peak area with average blank subtraction from empty graphite boats (Technique A), peak area with integrated background correction (Technique B), and peak height with averaged background correction (Technique C). Despite being the simplest to implement, subtracting the average background signal from the height of the peak produced during the vaporization step, i.e., Technique C, systematically yields the lowest detection limits without compromise in accuracy or precision.

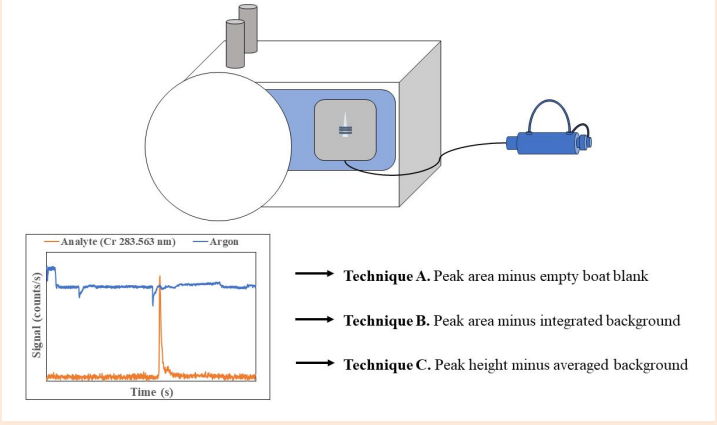

INTRODUCTION

Electrothermal vaporization (ETV) provides an efficient sample introduction pathway for spectrometric analytical techniques, including inductively coupled plasma (ICP) spectrometers. The idea of introducing dry vapour to the plasma source was proposed by early-ICP researchers Date and Gray,[1] which became a competitive alternative to conventional pneumatic nebulization. The immediate advantages of ETV systems, including the reduction of interferences and increased sample introduction efficiency, spurred rapid development into ETV within the scientific community; from 1990 to 2000, the rate of ETV-ICP mass spectrometry (MS) publications increased by 25 times.[2]

Despite its early success, the popularization of ETV has considerably stalled, in part due to the maturation of solution sampling (*e.g.*, addition of ultrasonic nebulizers) and other solid-sampling technologies (*e.g.*, laser ablation or laser induced breakdown spectroscopy). Furthermore, some features that were initially recognized as being unique to ETV (such as polyatomic interference management) have been met by advancements in ICPMS, including the addition of collision/reaction cells. Consequentially, other techniques became easier to use and operate, while ETV still demands careful optimization, operation complexity, and manual data processing. Data processing of transient signals is a particular limitation; in many versions of data collection software (such as Smart Analyzer Vision, the basic software for the SPECTRO ARCOS ICPOES instrument), automated background correction and other data processing are not possible. Within the past 10 years, automated data treatment has been made available through internal licensed software

including SPECTRO Smart Chrom Pro (SPECTRO AMETEK, Germany) or Thermo iTEVA (Thermo Scientific, USA). These software have been used to complete background corrections and peak integrations of signals in ETV-ICPOES data sets.[3–6] However, these programs require expensive licenses and have been criticized for slow data transfer rates and overall processing.[3] Functionality of ICPOES software is also criticized to be limited (particularly when compared to transient data processing software for ICPMS), potentially requiring export to external software for additional processing.[3] Some examples of external software for data processing include Excel and MATLAB. In a study by Chaves *et al.*,[4] a MATLAB script was developed to perform offline processing of ETV-ICPOES transient signals and was successfully applied for the determinations of Ca in bone ash and rice flour. Excel is used commonly for both ETV-ICPMS and ETV-ICPOES transient signal processing.[5–9] External software is readily-accessible and may allow for greater flexibility and customized data corrections.

ETV-ICPOES is valuable for the analysis of small sample phases (0.1-5 mg of solids or 5-40 µL of solutions or slurries)[2] and sensitive detections of trace elements. Recently, ETV-ICPOES has demonstrated success in trace forensic and archaeological analyses of hair,[10] solder,[11] ancient glasses,[12] avian bone,[13] and automotive paint.[14] Methods by ETV-ICPOES have also been developed for the multi-elemental analysis of environmental samples including soil,[15] plants,[16–18] and fly ash.[19–21] As noted by Aramendia *et al.*,[2] ETV-ICPOES is specially reserved for challenging analytical applications that are not easily achieved through other analytical methods. To stay competitive, increased support for method development and data processing, in addition to a stronger theoretical base, is needed.

Throughout an ETV temperature program, changes in temperature of the graphite furnace may affect the plasma in different ways. For instance, instantaneous heating of the furnace may increase the gas pressure and, in turn, the transport flow. When the ETV effluent is introduced into the plasma, a sample loading effect may be observed through a decrease in plasma brightness and suppression of Ar emission (Fig. 1). This signal suppression is proportional to sample mass.[15] To compensate for these effects, point-by-point internal standardization may be done by dividing the raw analyte signal by the signal of an Ar emission line at the same time. This strategy was shown to improve the linearity of the calibration curve and permit the integration of otherwise negative signals due to sample loading.[22] Internal standardization may also correct for signal drift. By using an Ar emission line that is monitored concurrently to analytes, a user may avoid using a solid or liquid internal standard, which would need to be carefully and uniformly mixed with the sample prior to introduction into the ETV furnace.

Blank subtraction is another procedure that is widely used. This

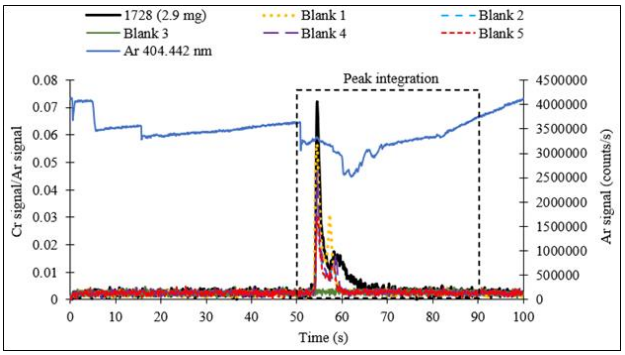

Fig. 1 Technique A of data processing. The Cr I (283.563 nm) signal is shown after internal standardization for a 2.9 mg sample of NIST CRM 1728 Tin-Alloy and five blanks (empty graphite boats). The average peak integration of the blanks is subtracted from the Cr peak area collected from an equal integration window (*e.g.*, 50-90 s).

involves measuring a material with the same matrix composition as the sample, less any analyte, and subtracting the integrated blank signal from the sample signal. In theory, the use of a blank would negate matrix interferences on the transient signal, but the problem becomes obtaining an appropriate blank that would exert the same matrix influence as a normal sample would. In cases of solid sampling, this is often not possible to obtain or recreate synthetically. As one alternative, Verrept *et al.*[23] proposed a "zero-mass signal" approach; this involves the analysis of empty boats as blank measurements. This was adapted for the direct solid-sampling of silicon carbide,[24] biological materials (such as fruit leaves,[25-27] wheat flour and sea lettuce[28]), and environmental samples (sewage and sediment[28]). Empty graphite boats can also be useful to monitor memory effects. However, in recent works, the empty-boat blank was criticized to not be a true blank for the analysis of solids and has been observed to vary greatly among replicate measurements.[29] Due to the presence of contamination in empty graphite boats, using an empty boat for blank subtraction was demonstrated to consistently decrease total signal integration and result in negative signal integrations for trace determinations with high background.[22, 29] The blank value was also seen to increase during an analysis series, attributed to memory effects.[30]

Background (or baseline) correction has been applied as an alternative to blank subtraction, where the average background signal measured before and/or after the vaporization peak is systematically subtracted from the analyte peak before integrating.[22, 29] This technique is especially useful in cases where an accurate blank cannot be obtained (e.g., for forensic solid samples such as solder or hair) or when a high signal background is present. For the determination of F using H_2 reaction gas in ETV, which greatly increased the background signal through the creation of a mixed-gas plasma, this approach improved the detection limit (defined as 3 times the standard deviation of the blank signal divided by the slope of the calibration curve) up to

250-fold (using the most sensitive emission line) versus that obtained with the blank subtraction approach based on empty graphite boats. [22] However, this apparent large improvement may be a spurious effect of computing the LOD using the standard deviation from the average *peak height* and the slope of the calibration curve obtained by plotting *peak area* of the vaporization peak versus analyte mass.

The goal of this work was to compare the common blank subtraction approach, Technique A (peak area with blank subtraction), to two data processing approaches that have not been previously used with ETV-ICPOES, Technique B (peak area with integrated background correction) and Technique C (peak height with averaged background correction), to find the one providing the best absolute detection limits for the multi-elemental analysis of solder by ETV-ICPOES without jeopardizing accuracy and precision. These techniques will be demonstrated on data sets from Pb-Sn and Pb-free solders collected from two published methods of solder analysis: MacConnachie *et al.*[11] and Moghadam *et al.*[29] This proof of concept will show that these new techniques involving background correction improve detection limits, a critical figure of merit for trace forensic applications, thus making ETV-ICPOES more competitive as an analytical technique. Their effect on accuracy, precision and sensitivity will also be examined.

EXPERIMENTAL

Instrumentation and software. All transient data sets of solders were obtained using an ETV system (ETV 4000C, Spectral Systems, Fürstenfeldbruck, Germany) coupled to an ICPOES (lateral plasma view SPECTRO ARCOS, SPECTRO Analytical Instruments, Kleve, Germany) instrument. The operating conditions (detailed in Table 1) are shared among two methods of solder analysis, which are based a previous ETV-ICPOES optimization for the analysis of stainless steels.[31] Transient signal collection was performed using Smart Analyzer Vision software (Version 6.01.0948). Data processing was done offline and manually using Microsoft Excel (Version 2309) for Microsoft 365.

Standard reference materials, gases, analytes. The three data processing techniques were demonstrated separately on two methods of solder analysis, which each involved a five-point external calibration with increasing mass aliquots of a certified reference material (CRM) from the National Institute of Standards and Technology (NIST, Gaithersburg, MD, USA). Information on both methods, including a list of analyte emission lines and details of the calibration, can be found in Table 2. Various matrix-matched CRMs were analyzed, depending on the method, to demonstrate accuracy and precision: for MacConnachie *et al.*,[11] C2416 Bullet Lead (NIST, Gaithersburg, MD, USA) was used as a matrix-matched sample for Pb-rich solders. For the method by Moghadam *et al.*,[29] the following Pb-free solders were used: 74X E F batch F, 74X HA G batch G, and 74X TC batch F (ARMI MBH Analytical LTD, Barnet, England).

Table 1. Instrument operating parameters for both methods of solder analysis, based on the optimization from Scheffler *et al.*[31]

ICP	
Radio-frequency power (KW)	1.70
Ar plasma gas flow rate (L min^{-1})	14.5
Auxiliary gas flow rate (L min^{-1})	1.50
Integration time (ms)	10
Sampling rate (Hz)	10
Observation height (mm)	10
ETV	
Ar bypass gas flow rate (L min^{-1})	0.5
Ar carrier gas flow rate (L min^{-1})	0.15
CF_4 reaction gas flow rate (mL min^{-1})	8.00
Temperature programming – Analysis (temperature, duration)	Initial (21 °C, 15 s), Pyrolysis (400 °C, 20 s), Cooling (No heating, 15 s), Vaporization (2300 °C, 30 s), Cooling (No heating, 20 s)
Temperature programming – Cleaning (temperature, duration)	Initial (21 °C, 0 s), Cleaning (2300 °C, 45 s), Cooling (No heating, 15 s)

Ultra-high purity argon (99.996% purity, liquid in Dewar, MEGS Specialty Gases, Ottawa, ON, Canada) was used for the plasma and auxiliary gases for the ICP and as bypass and carrier gases for the ETV furnace. Carbon tetrafluoride (MEGS Specialty Gases) was used as the reaction gas for ETV.

Graphite boat handling and cleaning. Before any analysis, graphite boats were cleaned using a temperature program described in Table 1. Boats were further wiped with a clean Q-tip to remove any remaining visible residue. To obtain a blank used for blank subtraction (Technique A), a clean empty boat was manually loaded into the graphite furnace using tweezers. This

Table 2. Solder methods used in this research

	Method by MacConnachie *et al.*[11]	Method by Moghadam *et al.*[29]
Calibration standard material	NIST 1131 Solder (40Sn-60Pb)	NIST 1728 Tin Alloy (Sn-3Cu-0.5Ag)
Calibration strategy	5-point external calibration (0.5-2.5 mg)	5-point external calibration (1.0-3.0 mg)
Ar line for internal standardization	Ar I (763.511 nm)	Ar I (404.442 nm)
Element lines monitored	Ag I (328.068 nm), Ar I (763.511 nm), As I (189.042 nm), Bi I (223.061 nm), Cu I (324.754) nm, Sb I (217.581 nm), Sn II (175.790 nm), and Pb II (172.680 nm)	Ag I (328.068 nm), Ar I (404.442 nm), As I (189.042 nm), Bi I (223.061 nm), Cr (283.563 nm), Cu I (324.754 nm), Fe I (373.486 nm), Sb I (217.581 nm), Sn II (175.790 nm), and Pb II (172.680 nm)

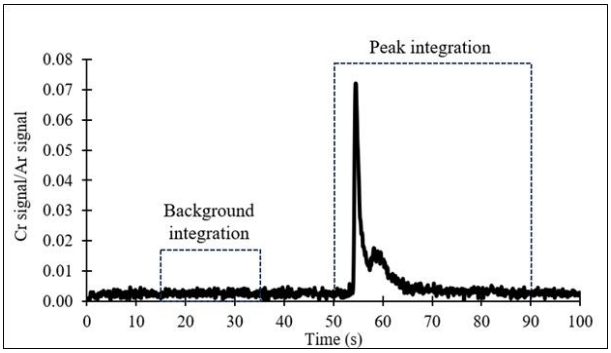

Fig. 2 Technique B of data processing. The Cr I (283.563 nm) signal is shown after internal standardization for a sample of NIST 1728 Tin-Alloy (2.9 mg). A factor of the background integration (to match the Cr integration window) is subtracted from the Cr peak area.

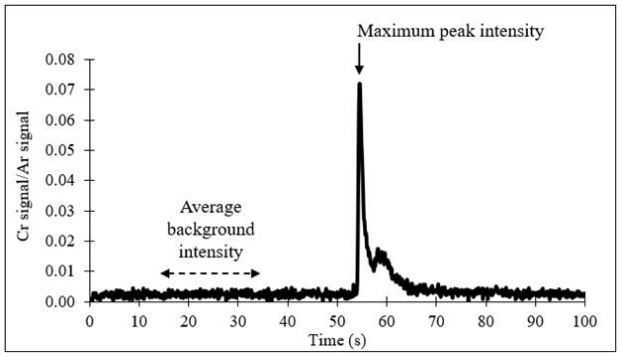

Fig. 3 Technique C of data processing. The Cr I (283.563 nm) signal is shown after internal standardization for a sample of NIST 1728 Tin-Alloy (2.9 mg). The average background intensity is subtracted from the Cr peak height.

was repeated with different graphite boats to give n=5 replicate blank measurements. Blank measurements were obtained at the start of analysis before sample or standard measurements.

Data processing. First, point-by-point internal standardization was carried out using Ar I (404.442 nm) or Ar I (763.511 nm), depending on the method. Then, different data processing techniques for blank subtraction and background correction were compared. Blank subtraction of the average integrated signal from five empty graphite boats (Fig. 1) constituted Technique A. Although the vaporization step lasted 30 s, a 40 s integration period was defined from 50-90 s to budget for short delays in the emergence of the vaporization peak, which could vary between replicates, and for some analyte peaks being broader (such as when analyte concentration is high). Because the ETV and ICPOES instruments did not operate synchronously, transient signal collection was initiated on the ICPOES software *before* starting the ETV temperature program. Small variations in temperature ramping of the furnace to vaporization temperatures could also occur, affecting when the vaporized analyte reached the ICP.

Technique B involved integrating a period of the background and subtracting this from sample peak integrations (Fig. 2). This background was selected as a period from 15-35 s, corresponding to the pyrolysis stage, to reflect the behaviour of the background during sample heating. The signal during this period was consistently flat and did not largely differ from the signal during cooling before the analyte peak, as can be seen for different elements in Pb-rich and Pb-free solders in Figs. S1- S10. However, because the time before an analyte peak may slightly vary, as explained earlier, data processing would have been further complicated if the cooling period had been used. Thus, the integrated signal during the 15-35 s period was further multiplied by 2 to match the integration width of the vaporization peak integration (40 s, from 50-90 s).

Technique C involved subtracting the average signal of the background interval from each point of the transient signal and measuring the resulting peak height (Fig. 3). The peak intensity of analyte signals, in other words, the maximum background-corrected signal during the vaporization window, was then correlated to analyte mass to produce the calibration curve. Technique C did not rely on integrations of the background or analyte peaks.

Limit of detection (LOD). The limit of detection (LOD) provides a useful figure of merit in evaluating analytical data and assessing the significance of trace quantifications. By definition, the LOD (or detection limit) is the lowest quantity or concentration of an analyte that can be detected. This provides a distinction between analyte detected in a sample *with certainty*, versus signal that is detected in a substance with no analyte, known as the blank. For Technique A, the common calculation of LOD (in units of mg) as three times the standard deviation of the blank signal (in arbitrary units (a.u.) after internal standardization with an Ar emission line), divided by the slope of the calibration curve (in a.u. mg^{-1}) was used (see Table S1 and Calculation S1 for an example).

When a background interval was used instead for correction, the standard deviation of the blank signal was replaced by the standard deviation of the background integrations (in a.u.) for Technique B (see Table S2 and Calculation S2 for an example), or the standard deviation of the background signal intensities (in a.u.) for Technique C (see Table S3 and Calculation S3 for an example), from five calibration standards (n=5).

RESULTS AND DISCUSSION

Effect of data processing on signal-to-background ratio and detection limit. Using the method by Moghadam *et al.*,[29] signals after blank subtraction (Technique A) or background corrections (Techniques B and C) are compared to signals by internal standardization alone in Fig. 4. For every element, Technique C

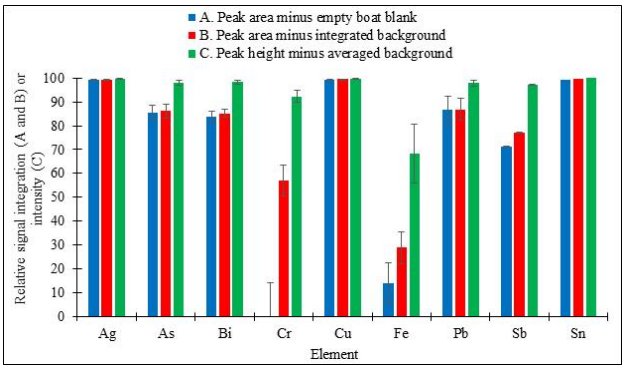

Fig. 4 Effects of data processing techniques on signal integrations (Techniques A and B) and signal intensities (Technique C) from samples of NIST 1728 Tin-Alloy (2.1-2.5 mg, n=5). Signals are mass-corrected and shown relative to signal by internal standardization alone. Data obtained using solder method by Moghadam *et al.*[29]

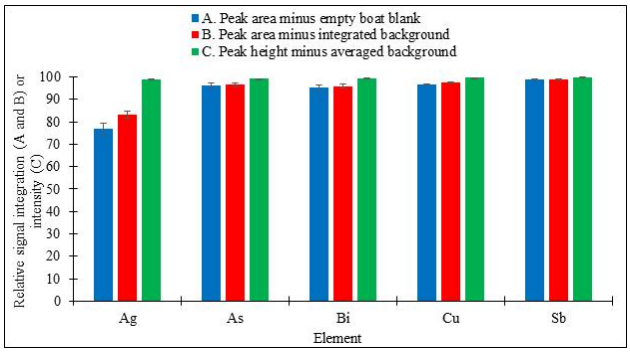

Fig. 5 Effects of data processing techniques on signal integrations (Techniques A and B) and signal intensities (Technique C) from samples of NIST C2416 Bullet Lead (1.5-2.1 mg, n=5). Signals are mass-corrected and shown relative to signal by internal standardization alone. Data obtained using solder method by MacConnachie *et al.*[11]

results in the highest relative signal. Notably, Technique A results in the lowest integration for Fe (~14% of signal by internal standardization alone) and negative signal for Cr (not shown). These elements are of the lowest concentrations within CRM NIST 1728 Tin-Alloy. The blank signals gathered during blank measurement likely contained contamination resulting in falsely low, and in few cases, negative signal integrations for these elements. This is visible in Fig. 1, where some blank signals exceed the sample signal. Although blank signals are expected to vary due to the condition of the boat, cleanliness of the graphite furnace, and handling procedures, to avoid a boat contamination issue going forward, graphite boats solely reserved for blanks could be used (instead of boats previously used for samples as done in this work). Such approach would allow an assessment of memory effects originating from the graphite tube or elsewhere (such as the transfer line). For the alloying elements including Sn (96.3% m/m), Ag (0.4591% m/m), and Cu (3.06% m/m), the effects of Techniques A-C were comparable and minimal. These elements produced the greatest signal-to-background ratio, and so the effect of correction was negligible as seen by the high relative signals (>99%). The effects of data processing techniques on signals are consistent when applied to the method by MacConnachie *et al.*,[11] as seen in Fig. 5: for every element studied, Technique C results in the highest relative signal.

The absolute detection limits calculated by each data processing technique are compiled in Table 3 for the two solder analysis methods. Irrespectively of the method, the lowest LODs generally resulted with Technique C. For the method by Moghadam *et al.*,[29] the improvement in detection limits by using background correction techniques can be visualized in Fig. 6 comparing the ratio of LODs from the technique of blank subtraction with the alternative techniques. As shown, LODs are improved when using background correction techniques, with the greatest improvements resulting from Technique C (between 1-3 orders of magnitude). These findings relate to those in Fig. 4 as lower detection limits are consistent with greater signal intensities.

Effect of data processing on accuracy. The results for three certified tin-base lead-free solder CRMs are presented in Table 4 (Cr was excluded because its concentration is not certified in there

Table 3. Absolute detection limits (ng) of analytes by three data processing techniques for two solder methods

Analyte	Technique A. Peak area minus empty boat blank		Technique B. Peak area minus integrated background		Technique C. Peak height minus averaged background	
	Pb-free solder[29]	Pb-rich solder[11]	Pb-free solder[29]	Pb-rich solder[11]	Pb-free solder[29]	Pb-rich solder[11]
Ag I (328.068 nm)	20	3	3	0.7	0.5	0.05
As I (189.042 nm)	5	8	1	7	0.1	7
Bi I (223.061 nm)	6	10	3	10	0.3	1
Cr I (283.563 nm)	10	N.D.*	0.1	N.D.	0.01	N.D.
Cu I (324.754 nm)	200	10	10	4	3	0.2
Fe I (373.486 nm)	30	N.D.	8	N.D.	0.3	N.D.
Pb II (172.680 nm)	20	800	20	1000	2	500
Sb I (217.581 nm)	20	10	3	10	0.3	2
Sn II (175.790 nm)	3000	300	2000	100	400	200

*Not determined

Table 4. Concentrations in % m/m, of elements in various certified tin-base lead-free solders obtained by different data processing techniques applied to solder method by Moghadam *et al.*[29] Certificate estimates reported with sample standard deviation, concentrations for Techniques A-C expressed as an average ± standard deviation (n varies)

CRM	Analyte	Certificate value	Technique A. Peak area minus empty boat blank	Technique A. Peak area minus integrated background	Technique A. Peak height minus averaged background
74X E F	Ag	0.667 ± 0.006 (9)	0.64 ± 0.12 (5)	0.57 ± 0.14 (5)	0.54 ± 0.14 (5)
	As	0.0092 ± 0.0014 (11)	0.0090 ± 0.0019 (5)	0.0092 ± 0.0024 (5)	0.0111 ± 0.0034 (5)
	Bi	0.0099 ± 0.0013 (11)	0.0090 ± 0.0023 (5)	0.0089 ± 0.0024 (5)	0.0079 ± 0.0027 (5)
	Cu	2.94 ± 0.04 (12)	2.63 ± 0.37 (5)	2.63 ± 0.37 (5)	2.66 ± 0.38 (5)
	Pb	0.0248 ± 0.0016 (12)	0.0276 ± 0.0068 (5)	0.0251 ± 0.0075 (5)	0.0262 ± 0.0063 (5)
74X HA G	As	0.0032 ± 0.0011 (11)	0.00295 ± 0.00095 (5)	0.00256 ± 0.00073 (5)	0.00259 ± 0.00041 (5) §
	Bi	0.0639 ± 0.0018 (12)	0.0489 ± 0.0088 (5) §	0.0480 ± 0.0087 (5) §	0.062 ± 0.012 (5)
	Fe	0.0029 ± 0.0004 (11)	0.013 ± 0.007 (3) *	0.0057 ± 0.0027 (5)	0.0049 ± 0.0012 (5) §
	Pb	0.077 ± 0.004 (11)	0.084 ± 0.020 (5)	0.074 ± 0.017 (5)	0.070 ± 0.012 (5)
	Sb	2.1 ± 0.03 (12)	2.35 ± 0.76 (5)	2.20 ± 0.71 (5)	3.3 ± 1.4 (5)
74X TC	Ag	0.0391 ± 0.0025 (12)	0.0368 ± 0.0075 (5)	0.0370 ± 0.0076 (5)	0.051 ± 0.015 (5)
	As	0.024 ± 0.003 (9)	0.0317 ± 0.0075 (5)	0.0304 ± 0.0073 (5)	0.032 ± 0.010 (5)
	Bi	0.106 ± 0.004 (11)	0.0891 ± 0.0062 (5) §	0.0874 ± 0.0061 (5) §	0.101 ± 0.011 (5)
	Cu	4.99 ± 0.06 (12)	4.73 ± 0.80 (5)	4.72 ± 0.80 (5)	4.14 ± 0.70 (5)
	Fe	0.0031 ± 0.0006 (12)	0.022 ± 0.015 (3) *	0.0066 ± 0.0019 (5) §	0.0054 ± 0.0030 (5)
	Pb	0.183 ± 0.004 (12)	0.246 ± 0.058 (5)	0.226 ± 0.053 (5)	0.220 ± 0.030 (5)
	Sb	0.124 ± 0.002 (12)	0.138 ± 0.020 (5)	0.110 ± 0.016 (5)	0.140 ± 0.026 (5)

* Negative estimates obtained and removed before average calculation
§ Not in agreement with certificate value (Student's t-test, 95% confidence interval, $p < 0.05$)

Table 5. Concentrations, in % m/m, of elements in SRM C2416 obtained by different data processing techniques applied to solder method by MacConnachie *et al.*[11] Certificate values reported with estimated uncertainty, concentrations for Techniques A-C expressed as an average ± standard deviation (all n=5)

Analyte	Certificate value	Technique A. Peak area minus empty boat blank	Technique B. Peak area minus integrated background	Technique C. Peak height minus averaged background
Ag	0.0044 ± 0.0002	0.00298 ± 0.00045 §	0.00315 ± 0.00045 §	0.00388 ± 0.00064
As	0.056 ± 0.001	0.0624 ± 0.0052	0.0625 ± 0.0054	0.0583 ± 0.0033
Bi	0.10 ± 0.01	0.108 ± 0.013	0.108 ± 0.013	0.113 ± 0.0026
Cu	0.065 ± 0.002	0.0487 ± 0.0082 §	0.0474 ± 0.0080 §	0.0491 ± 0.0026
Sb	0.79 ± 0.01	0.818 ± 0.068	0.819 ± 0.068	0.839 ± 0.097

§ Not in agreement with certificate value (Student's t-test, 95% confidence interval, $p < 0.05$)

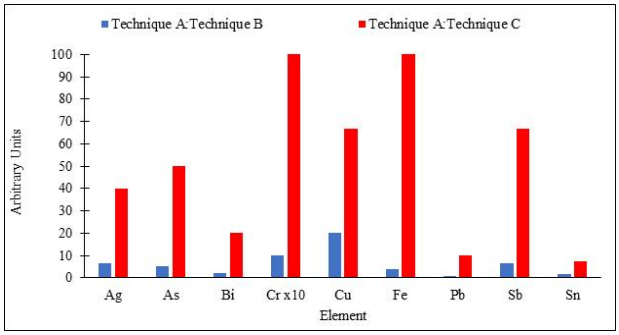

Fig. 6 Ratios of detection limits by element between data processing techniques. Results obtained using solder method by Moghadam *et al.*[29]

CRMs). Using Technique C, the most element concentrations agreed with certificate concentrations (Student's t-test at the 95% confidence interval, p = 0.053-0.74); the only exceptions are As and Fe in material 74X HA G (p = 0.028 and 0.020, respectively). However, the measured concentrations for As and Fe are not significantly different from those measured by Technique B; the disagreement with the certified values stems from the higher precision achieved for those elements by Technique C for this specific sample. Better precision was not achieved by Technique C for the other two CRMs. Technique A achieved similar levels of agreement in many elements (p = 0.063-0.83) except for Bi in 74X HA G (p = 0.019) and 74X TC (p = 0.0032). However, several negative estimates were obtained by Technique A only, resulting in fewer replicate measurements used for averaged Fe concentrations. Boats reserved for blanks, repeating cleaning cycles, or using a higher temperature than the vaporization temperature during the cleaning step may reduce this issue. Technique B did not produce accurate concentrations for Bi in 74X HA G and 74X TC (p = 0.015 and 0.0021, respectively) or Fe in 74X TC (p = 0.015) but the measured concentrations for all other elements agreed with certified values (p = 0.081-0.99). The results for a Pb-rich material, NIST C2416 bullet lead, were found following the method by MacConnachie *et al.*[11] As can be seen in Table 5, Technique C produced concentrations in agreement with certificate values for all studied elements (p = 0.089-0.32).

Table 6. Relative standard deviations (RSDs) and standard errors (SEs) of element concentrations in certified solders using different data-processing techniques. RSDs and SEs are presented as a range from minimum to maximum value, with the median shown in italics

CRM	RSDs, %			SEs, % m/m		
	Technique A. Peak area minus empty boat blank	Technique B. Peak area minus integrated background	Technique C. Peak height minus averaged background	Technique A. Peak area minus empty boat blank	Technique B. Peak area minus integrated background	Technique C. Peak height minus averaged background
			Sn-based Pb-free solder CRMs			
74X E F	14-26, *22*	14-30, *26*	14-35, *26*	0.00087-0.16, *0.0031*	0.0011-0.16, *0.0034*	0.0012-0.17, *0.0028*
74X HA G	18-56, *32*	18-47, *28*	10-42, *25*	0.0040-0.0090, *0.0041*	0.0012-0.0076, *0.0025*	0.00055-0.0056, *0.0029*
74X TC	7-68, *22*	7-28, *22*	11-55, *30*	0.0028-0.0257, *0.0059*	0.0008-0.024, *0.0033*	0.0013-0.037, *0.0058*
			Pb-rich solder CRM			
C2416	8-17, *12*	8-17, *12*	5-16, *10*	0.00020-0.030, *0.0037*	0.00020-0.030, *0.0036*	0.00029-0.053, *0.0050*

Technique A concentrations agreed for As, Bi, and Sb ($p = 0.051$-0.41), but not for Ag and Cu ($p = 0.0021$ and 0.0045, respectively). Similarly, Technique B produced concentrations in agreement for all elements ($p = 0.055$-0.40) except for Ag and Cu ($p = 0.0034$ and 0.0040, respectively). Thus, Technique C provides better accuracy despite variations in peak shape between elements depending on analyte concentration and the matrix (Figs. S1- S10). Technique C is also being the simplest to implement. The fact that accurate results were generally obtained indicates the absence of interference.

Relative standard deviation (RSD) and standard error (calculated as $SE = \sigma/(\sqrt{n})$, where σ is the sample standard deviation of n replicate estimates) were used as measures of precision when evaluating data processing techniques. The observed ranges of RSDs and SEs for samples are shown in Table 6. For both solder methods, RSDs were found to be consistent among techniques when compared element-by-element and are of the expected range for direct solid analyses by ETV (between 10-15%[30] and up to 30% for heterogenous materials[15]). Paired Student's t-tests comparing independent single results (*i.e.*, RSDs of elements in a material) further indicate no significant differences among any combination of technique (Technique A versus Technique B, Technique A versus Technique C, and Technique B versus Technique C), for any material studied. The highest RSDs exceeding 50% were obtained only for Technique A in cases where fewer than 5 replicates were available. No major differences in SEs were observed among techniques, inferring equal sample variability between techniques.

CONCLUSION

For the first time, this work compared the conventional blank subtraction technique using an empty graphite boat to two background correction techniques for offline data processing of solder samples by ETV-ICPOES. These techniques are useful for users of ETV technology, including users of the ETV-4000 by Spectral Systems (the only commercially available model of an ETV furnace). A comparison of these techniques on two methods of solder analysis demonstrated that simple changes in data processing can result in improvements in figures of merit without modifying the instrumental set-up, method parameters, or completing additional optimization. When using the common approach, peak area with blank subtraction of empty boats (Technique A), the largest reduction in signal integration (and thus, loss of sensitivity) is observed among elements, as well as the highest detection limits. The greatest reduction in signal is seen for trace elements (at mg kg^{-1} level), even resulting in negative signals when blank signals are collected from contaminated graphite boats. The lowest detection limits are observed using peak height with averaged background correction (Technique C), where the highest relative signals were also obtained after correction (Fig. 4). Furthermore, comparison of measured concentrations with certified values indicated generally better accuracy with Technique C for two different types of solder (Pb-free and Pb-rich). Techniques A and B provided inaccurate results for only a few elements according to Student's t-tests. No differences in relative standard deviations or standard errors were observed among Techniques, but the highest RSDs (>50%) were found when using Technique A.

Users of ETV-ICPOES should consider detection limits, analyte concentrations in samples, and signal-to-background ratios or spectral background before implementing a data processing strategy or combination of strategies. This works demonstrates that, for trace or ultra-trace determinations, users may consider using peak heights (Technique C) for the lowest detection limits (by up to three orders of magnitude) without jeopardizing accuracy and precision. Technique B (peak area with integrated background correction) or C would compensate for high spectral background, which would otherwise cause negative peak integrations by Technique A. Further, users may favour Technique B or C as these methods do not require the additional analysis of empty graphite boats, thus limiting analysis time and increasing the lifetime of graphite boats. While the temperature program is relatively short, there are other added time considerations from extra analyses, which would impact long-term routine analysis: users must wait for the graphite boats to cool

down for safe handling and must process extra transient data files. In any case, the use of an empty graphite boat should not be considered as a suitable blank for some solid-sampling applications. Future work will investigate the effect of Technique C on the linear dynamic range and will check the performance of Techniques B and C for the analysis of other materials. The long-term stability of Techniques will also be tested.

ASSOCIATED CONTENT

Supporting information (Tables S1−S3, Calculations 1−3, and Figs. S1−S10) is available at www.at-spectrose.com/as/home.

AUTHOR INFORMATION

Diane Beauchemin received her Ph.D. in 1984 from Université de Montréal. She is a professor (Full) at Queen's University. Her research efforts are focused on inductively coupled plasma mass spectrometry (ICPMS) and ICP optical emission spectrometry (OES) from both fundamental and application perspectives, and expanding the range of application of ICPMS/OES to geochemical exploration, risk assessment of food safety, characterization of nanoparticles, and forensic analysis. She has been working as member of editorial board for *Atomic Spectroscopy*. Diane Beauchemin won the Alan Date Memorial Award (1988) from VG Elemental, the Distinguished Service Award (2001) from Spectroscopy Society of Canada, the Maxxam Award (2017) and Clara Benson Award (2019) from Canadian Society for Chemistry, and the Gerhard Herzberg Award (2018) from the Canadian Society for Analytical Sciences and Spectroscopy. She is author or co-author of over 160 articles published in peer-reviewed scientific journals.

Corresponding Author

*D. Beauchemin

Email address: diane.beauchemin@queensu.ca

Notes

The authors declare no competing financial interest.

ACKNOWLEDGMENTS

The authors gratefully acknowledge the financial support of the Natural Sciences and Engineering Research Council of Canada (RGPNM 39487-2018). KM is grateful to Queen's University School of Graduate Studies for graduate awards.

REFERENCES

1. A. R. Date and A. L. Gray, *Spectrochim. Acta B*, 1983, **38**, 29–37. https://doi.org/10.1016/0584-8547(83)80100-1
2. M. Aramendía, M. Resano and F. Vanhaecke, *Anal. Chim. Acta*, 2009, **648**, 23–44. https://doi.org/10.1016/j.aca.2009.06.027
3. A. Limbeck, M. Bonta, and W. Nischkauer, *J. Anal. At. Spectrom.*, 2017, **32**, 212–232. https://doi.org/10.1039/C6JA00335D
4. E. S. Chaves, S. Compernolle, M. Aramendía, E. Javierre, E. Tresaco, M. T. C. De Loos-Vollebregt, A. J. Curtius, and F. Vanhaecke, *J. Anal. At. Spectrom.*, 2011, **26**, 1833–1840. https://doi.org/10.1039/c1ja10083a
5. A. Martin-Esteban, B. Slowikowski, and K. H. Grobecker, *Talanta*, 2004, **63**, 667–673. https://doi.org/10.1016/j.talanta.2003.12.011
6. C. Hommel, J. Hassler, R. Matschat, T. Vogt, A. K. Detcheva, and S. Recknagel, *J. Anal. At. Spectrom.*, 2021, **36**, 1683–1693. https://doi.org/10.1039/D1JA00081K
7. G. Ertas and J. A. Holcombe, *J. Anal. At. Spectrom.*, 2005, **20**, 687–695. https://doi.org/10.1039/b505482f
8. F. Vanhaecke, M. Verstraete, L. Moens, and R. Dams, *Anal. Commun.*, 1999, **36**, 89–92. https://doi.org/10.1039/a809318k
9. A. Rowland, T. B. Housh, and J. A. Holcombe, *J. Anal. At. Spectrom*, 2008, **23**, 167–172. https://doi.org/10.1039/B709089G
10. M. MacConnachie, S. Lu, Y. Wang, J. Williams, and D. Beauchemin, *RSC Adv.*, 2022, **12**, 27064–27071. https://doi.org/10.1039/D2RA05654B
11. M. MacConnachie, K. Moghadam, and D. Beauchemin, *J. Anal. At. Spectrom.*, 2021, **36**, 1600–1606. https://doi.org/10.1039/D1JA00172H
12. A. Detcheva, J. Hassler, and R. Georgieva, *Anal. Lett.*, 2012, **45**, 603–612. https://doi.org/10.1080/00032719.2011.649463
13. M. MacConnachie, M. Lapointe, E. Galiano, and D. Beauchemin, *J. Anal. At. Spectrom.*, 2020, **35**, 2487–2493. https://doi.org/10.1039/D0JA00288G
14. L. Huang and D. Beauchemin, *J. Anal. At. Spectrom.*, 2017, **32**, 1601–1607. https://doi.org/10.1039/C7JA00196G
15. A.-S. Masquelin, F. Kaveh, A. Asfaw, C. J. Oates, and D. Beauchemin, *Geochem. Explor. Environ. Anal.*, 2013, **13**, 11–20. https://doi.org/10.1144/geochem2012-129
16. P. Masson, *Spectrochim. Acta B*, 2014, **102**, 24–27. https://doi.org/10.1016/j.sab.2014.10.004
17. P. Masson, *J. Anal. At. Spectrom.*, 2011, **26**, 1290–1293. https://doi.org/10.1039/C0JA00156B
18. A. Detcheva, P. Barth, and J. Hassler, *Anal. Bioanal. Chem.*, 2009, **394**, 1485–1495. https://doi.org/10.1007/s00216-009-2835-4
19. A. Al Hejami and D. Beauchemin, *J. Anal. At. Spectrom.*, 2019, **34**, 1426–1432. https://doi.org/10.1039/C8JA00266E
20. G. Bauer and A. Limbeck, *Microchem. J.*, 2018, **137**, 496–501. https://doi.org/10.1016/j.microc.2017.12.017
21. Y. Zhang, Z. Jiang, and B. Hu, *Rapid Commun. Mass Spectrom.*, 2006, **20**, 2091–2098. https://doi.org/10.1002/rcm.2565
22. P. Maung and D. Beauchemin, *J. Anal. At. Spectrom.*, 2021, **36**, 1104–1111. https://doi.org/10.1039/D1JA00090J
23. P. Verrept, R. Dams, and U. Kurfürst, *Fresenius J. Anal. Chem.*, 1993, **346**, 1035–1041. https://doi.org/10.1007/BF00323712

24. A. Golloch, M. Haveresch-Kock, and F. Plantikow-Voβgätter, *Spectrochim. Acta B*, 1995, **50**, 501–516. https://doi.org/10.1016/0584-8547(94)00144-K
25. F. Vanhaecke, S. Boonen, L. Moens, and R. Dams, *J. Anal. At. Spectrom*., 1995, **10**, 81–87. https://doi.org/10.1039/ja9951000081
26. A. Virgilio, J. A. Nóbrega, J. F. Rêgo, and J. A. G. Neto, *Spectrochim. Acta B*, 2012, **78**, 58–61. https://doi.org/10.1016/j.sab.2012.09.003
27. P. Masson, M. Dauthieu, F. Trolard, and L. Denaix, *Spectrochim. Acta B*, 2007, **62**, 224–230. https://doi.org/10.1016/j.sab.2007.01.004
28. S. Boonen, F. Vanhaecke, L. Moens, and R. Dams, *Spectrochim. Acta B*, 1996, **51**, 271–278. https://doi.org/10.1016/S0584-8547(99)80004-4
29. K. Moghadam, C. Wheeler, and D. Beauchemin, *Atom. Spectrosc*., 2023, **44**, 123–130. https://doi.org/10.46770/AS.2023.113
30. L. Moens, P. Verrept, S. Boonen, F. Vanhaecke, and R. Dams, *Spectrochim. Acta B*, 1995, **50**, 463–475. https://doi.org/10.1016/0584-8547(94)00153-M
31. G. L. Scheffler, A. J. Brooks, Z. Yao, M. R. Daymond, D. Pozebon, and D. Beauchemin, *J. Anal. At. Spectrom*., 2016, **31**, 2434–2440. https://doi.org/10.1039/C6JA00369A